University of Nebraska - Lincoln

DigitalCommons@University of Nebraska - Lincoln

Nutrition and Health Sciences -- Faculty Publications

Nutrition and Health Sciences, Department of

2018

Effects of tunable, 3D-bioprinted hydrogels on human brown adipocyte behavior and metabolic function

Mitchell Kuss
University of Nebraska Medical Center, mitchell.kuss@unmc.edu

Jiyoung Kim
University of Nebraska - Lincoln

Dianjun Qi
University of Nebraska Medical Center

Shaohua Wu
University of Nebraska Medical Center, shaohua.wu@unmc.edu

Yuguo Lei
University of Nebraska-Lincoln, ylei14@unl.edu

See next page for additional authors

Follow this and additional works at: http://digitalcommons.unl.edu/nutritionfacpub

🌀 Part of the Human and Clinical Nutrition Commons, Molecular, Genetic, and Biochemical Nutrition Commons, and the Other Nutrition Commons

Authors

Mitchell Kuss, Jiyoung Kim, Dianjun Qi, Shaohua Wu, Yuguo Lei, Soonkyu Chung, and Bin Duan

Effects of tunable, 3D-bioprinted hydrogels on human brown adipocyte behavior and metabolic function

Mitchell Kuss[a,b], **Jiyoung Kim**[c], **Dianjun Qi**[a,d], **Shaohua Wu**[a,b], **Yuguo Lei**[a,e], **Soonkyu Chung**[c,*], and **Bin Duan**[a,b,f,*]

[a]Mary & Dick Holland Regenerative Medicine Program, University of Nebraska Medical Center, Omaha, NE 68198, USA

[b]Division of Cardiology, Department of Internal Medicine, University of Nebraska Medical Center, Omaha, NE 68198, USA

[c]Department of Nutrition and Health Sciences, University of Nebraska-Lincoln, Lincoln, NE 68516, USA

[d]Department of General Practice, The First Affiliated Hospital of China Medical University, Shenyang, Liaoning, People's Republic of China

[e]Department of Chemical and Biomolecular Engineering, University of Nebraska-Lincoln, Lincoln, NE 68516, USA

[f]Department of Surgery, College of Medicine, University of Nebraska Medical Center, Omaha, NE 68198, USA

Abstract

Obesity and its related health complications cause billions of dollars in healthcare costs annually in the United States, and there are yet to be safe and long-lasting anti-obesity approaches. Using brown adipose tissue (BAT) is a promising approach, as it uses fats for energy expenditure. However, the effect of the microenvironment on human thermogenic brown adipogenesis and how to generate clinically relevant sized and functioning BAT are still unknown. In our current study, we evaluated the effects of endothelial growth medium exposure on brown adipogenesis of human brown adipose progenitors (BAP). We found that pre-exposing BAP to angiogenic factors promoted brown adipogenic differentiation and metabolic activity. We further 3D bioprinted brown and white adipose progenitors within hydrogel-based bioink with controllable physicochemical properties and evaluated the cell responses in 3D bioprinted environments. We used soft, stiff, and stiff-porous constructs to encapsulate the cells. All three types had high cell viability and allowed for varying levels of function for both white and brown adipocytes. We found that the soft hydrogel constructs promoted white adipogenesis, while the stiff-porous hydrogel constructs improved both white and brown adipogenesis and were the optimal condition for promoting brown adipogenesis. Consistently, stiff-porous hydrogel constructs showed higher metabolic activities than stiff hydrogel constructs, as assessed by 2-deoxy glucose uptake (2-DOG)

*Corresponding authors at: Department of Nutrition and Health Sciences, University of Nebraska-Lincoln, Lincoln, NE 68516, USA (S. Chung); Mary & Dick Holland Regenerative Medicine Program, University of Nebraska Medical Center, Omaha, NE 68198, USA (B. Duan). schung4@unl.edu (S. Chung), bin.duan@unmc.edu (B. Duan).

and oxygen consumption rate (OCR). These findings show that the physicochemical environments affect the brown adipogenesis and metabolic function, and further tuning will be able to optimize their functions. Our results also demonstrate that 3D bioprinting of brown adipose tissues with clinically relevant size and metabolic activity has the potential to be a viable option in the treatment of obesity and type 2 diabetes.

Keywords

Tissue engineering; Brown adipocytes; Obesity; Stiffness; Porosity

1. Introduction

Obesity and its related health issues are major concerns in the United States health care system. The obesity-mediated health complications, such as type 2 diabetes mellitus (T2DM), cause $190 billion in healthcare costs annually in the United States [1]. One promising strategy for the treatment or prevention of obesity-mediated health complications is augmenting brown adi-pose tissue (BAT) thermogenesis. BAT is a specialized fat that actively disposes of glucose and fatty acids from circulation by dissipating the mitochondrial proton gradient into heat through uncoupling protein-1 (UCP1) [2,3]. Recent advances in our understanding of BAT in humans have provided a new insight into weight loss strategies, as well as metabolic improvement [4,5]. Humans possess a substantial amount of energy-burning brown/beige fat, especially in the neck and supraclavicular area [6,7]. It is estimated that brown/beige fat could be responsible for >20% of daily energy expenditure in healthy humans [8]. Since increased BAT mass/activity significantly improves glucose and lipid home-ostasis, BAT has garnered attention as a therapeutic intervention for obesity and T2DM [9]. However, activation or induction of BAT thermogenesis shows negative regulation with BMI, body fat content, visceral fat, age, and plasma glucose levels [10–14]. In addition, induction of BAT by a pharmacological dose of β3-agonists failed to help the weight loss of obese individuals [15–17]. It is worthwhile to notice that restoration of BAT by implanting BAT from healthy donor mice to diabetic recipient mice can effectively reverse T2DM and other metabolic disorders [18,19]. These results support that BAT transplantation is a promising and alternative approach to combat obesity and type 2 diabetes utilizing BAT energetics.

There are at least three different types of adipocytes found in humans: white adipocytes (WA) that are mainly involved in energy storage, classical brown adipocytes that share myogenic origin (myogenic factor 5 positive-Myf5^{+}), and beige adipocytes that have the same cellular origin as white adipocytes (Myf5^{−}) [20,21]. Beige adipocytes express transient levels of UCP1 upon external thermogenic stimuli, while classical brown adipocytes possess constitutively active UCP1 expression, suggesting an ideal cell preparation for transplantation [22,23]. The effects of physico-chemical microenvironments on white adipocyte culture [24] and white adipogenic differentiation of mesenchymal stem cells [25,26] have been widely studied. For example, Pellegrinelli et al. studied the role of mechanotransduction of the extracellular matrix on human WA, where a 3D decellularized extracellular matrix hydrogel was developed and a mechanical compression was applied to

the WA [27]. There are several studies on generating 3D beige adipocyte cultures using adipogenic mesenchymal stromal vascular cells or bone marrow-derived non-hematopoietic cells from humans [28]. By using murine adi-pose derived stem cells, Tharp et al demonstrated that the implantation of scaffold-assisted 3D-BAT successfully elevated core body temperature during cold challenges, improved glucose homeostasis, and reduced weight gain, compared to the hydrogel control[29]. However, very few studies have been conducted to generate 3D cultures from human classical brown precursor cells (BAP), due to the lack of appropriate cell models and difficulties in the isolation of human BAP. Considering the metabolic differences of human and rodent brown fat biology, it is an important gap to fill, because the implementation of BAT transplantation is a promising therapy for the treatment of obesity.

BAT is a highly innervated tissue with a well-organized vasculature system [30]. Maintenance of a capillary network is critically important for its metabolic function as well as survival of engrafted tissue. There is increasing evidence that angiogenic factors modulate the brown/beige differentiation and its survival after transplantation [31,32]. On the other hand, the microenvironment of the 3D culture conditions, such as stiffness or porosity of the matrix, have shown to affect the behavior of the white adipocytes [33–35]. Therefore, the modulation of both BAP and the matrix hydrogel formulation would be important factors to consider for generating metabolically active 3D BAT depots for implantation.

To obtain physiological relevance to humans, we used the BAP established from humans in comparison with white adipose progenitor cells (WAP) [36]. In this study, we first optimized the early differentiating conditions of human BAP into functional brown adipocytes (BA). By using the optimized culture conditions, our primary goal was to generate 3D bioprinted adipose constructs that have clinically relevant size and are applicable for implantation. Our study demonstrated that tuning the stiffness and porosity of an HA-based hydrogel matrix regulates the metabolic functions of 3D BAT. Our work will provide an important insight into implementing the 3D BAT strategy to potentiate the metabolic function in humans.

2. Materials and methods

2.1. Maintenance and differentiation of human white- and brown-progenitor cell-lines

Immortalized human WAP and BAP were a generous gift from Dr. Yu-Hua Tseng at the Joslin Diabetes Center, Harvard Medical School. In detail, primary stromal vascular cells, isolated from either subcutaneous fat or neck brown fat from one anonymous female (subject 5), were infected with retrovirus expressing hTERT [36]. The selected immortalized cells were grown and maintained in DMEM with 10% FBS and 1% Pen/Strep (Gibco). To optimize the brown differentiation potential, brown precursor cells were grown in either DMEM or endothelial growth medium (EGM) (Lonza) before differentiation. For adipocyte differentiation, we followed the published protocol [36].

2.2. Polymer modification and hydrogel bioink preparation

Photocrosslinkable hyaluronic acid (HA, NovaMatrix, ~1200 kDa) and gelatin (Gel, from bovine skin, Sigma) were synthesized as previously reported through the reaction of

methacrylic anhydride (Sigma) in deionized water [37]. For bioink preparation, methacrylated HA (Me-HA, 1.5%w/v), methacrylated gelatin (Me-Gel, 1.5%w/v), HA (3%w/v), and gelatin (3% w/v) were dissolved in cell culture medium with a cell suspension (5 10^6 cells/ml) and 0.05% w/v 2-hydroxy-1(4-(hydroxyethyl)phenyl)-2-methyl-1-propanone (Irgacure 2959; CIBA Chemicals). HA and gelatin, without modification, were used to increase the viscosity and printability and to maintain the softness of the bioprinted constructs for cell spreading.

2.3. 3D bioprinting and characterization of bioprinted constructs

Prior to 3D bioprinting, BAP were expanded with EGM medium, while white precursor cells were maintained in DMEM medium as described in 2.1. For the 3D bioprinting with the hydrogel bioinks, the gel precursors with cells were loaded into the deposition syringes (Nordson EFD) with 22G metal tips, extruded by the 3D bio-printer (3D Bioplotter, EnvisionTEC, Germany) based on the disc shaped design ($\varnothing$8 mm × 1.2 mm), and subsequently exposed to an OmniCure S2000 UV lamp (Lumen Dynamics) for 30 or 90 s at room temperature. The bioprinting pattern was printed as to make solid discs (denoted as soft solid and stiff solid), as well as in lines spaced 0.8 mm apart, as to create porous discs with 90 s photocrosslink (denoted as stiff porous) (Fig. 2A). The stiffnesses of the bioprinted hydrogel discs were measured using a compression tester (Agilent T150 UTM) at room temperature. The compressing speed was 5 mm/min, and the raw load was set to be 540 mN. For surface morphology observation, the bioprinted constructs were washed with deionized water and were lyophilized for 3 days then sputter coated with gold for SEM (FEI Quanta 200) imaging. The 3D printed stiff-porous constructs were also imaged by using a Zeiss Discovery v8 stereo microscope.

2.4. Differentiation of 3D WAP and BAP constructs

After bioprinting, all gels were placed in growth medium (GM) for one day. After that, the cell-laden constructs were placed in differentiation medium, consisting of DMEM with 2% FBS, 1% Pen/Strep, 0.5 μM recombinant human insulin (Alfa Aesar), and 2 nM tri-iodothyronine (T3, Sigma) for 6 days, with medium changed every 3 days. Induction was further conducted after 6 days of differentiation by using induction medium (IM) for another 12 days. Induction medium consisted of differentiation medium, 33 μM biotin (Sigma), 17 μM pantothenate (Sigma), 0.1 μM dexamethasone (Sigma), 500 μM 3-isobutyl-1-methyl xanthine (IBMX, Sigma), and 30 lM indomethacin (Sigma).

2.5. Cell viability

The viability and circularity of encapsulated cells was determined using a Live/Dead assay (Invitrogen) after differentiation and induction as previously described [38], and fluorescence images were obtained using a confocal laser scanning microscope (CLSM, LSM 710, Carl Zeiss). Cell viability was semi-quantitatively measured via counting live (green) and dead (red) cells based on Live/Dead images (at least six images were analyzed for each hydrogel sample), using ImageJ [39].

2.6. Immunofluorescence (IF) staining

For IF staining, the constructs were fixed in 4% paraformalde-hyde, permeabilized in 0.2% Triton X-100, and then blocked with 1% bovine serum albumin (BSA) overnight at 4 °C. The samples were incubated in the primary antibody to UCP1 (1:100, Abcam) overnight at 4 °C. Secondary fluorescent antibodies for UCP1 (1:100), and/or BODIPY® (10 μg/ml, Thermo Scientific) were incubated for 2 h, and nuclear counterstaining (via Draq 5, 1:1000, Biostatus) were performed for 30 min at room temperature. Then samples were imaged with a Zeiss 710 CLSM. Lipid droplets were identified as round structures that were stained by BODIPY®. The lipid density and lipid droplet size were measured and calculated by analyzing nine images from three samples using ImageJ software. Lipid density was calculated by comparing total lipid (green) area with total cells in the images.

2.7. Western blot

Total cell extracts were prepared as described previously [40]. Proteins were fractionated using 4–15% precast polyacrylamide gel (Bio-Rad) and transferred to PVDF membranes with a semi-dry transfer unit (Hoefer TE77X). Antibody targeting UCP1 (#14670), HDAC1(#34589), histone 3 (H3, 4499) and β-actin (4967) were purchased from Cell Signaling Technology. Blots were visualized with FluorChem™E imaging system (Protein Simple).

2.8. RNA isolation and quantitative real time polymerase chain reaction (qPCR)

For qPCR analysis, the samples were first homogenized in lysis buffer using a bead miller (Fisher Scientific). Total RNA was extracted from the cell-laden constructs using QIA-Shredder and RNeasy mini-kits (QIAgen), according to the manufacturers' instructions. Total RNA was synthesized into first strand cDNA in a 20 μL reaction using an iScript cDNA synthesis kit (BioRad Laboratories). Real-time PCR analysis was performed in a StepOnePlus™ Real-Time PCR System (Thermo Scientific) using SsoAdvanced SYBR Green Supermix (Bio-Rad). cDNA samples were analyzed for the gene of interest and for the housekeeping gene 18S rRNA. The level of expression of each target gene was calculated using the comparative Ct ($2^{-\Delta ct}$) method. For microRNA analysis, we followed the protocol that we have described previously [41].

2.9. Oxygen consumption rate (OCR)

To determine the mitochondrial respiration activities, the O_2 concentration in the cells was measured using XF24 extracellular flux analyzer (Seahorse) as we conducted previously [41]. Briefly, human BAP were seeded in gelatin-coated seahorse microplate (24-well) until reached confluence followed by brown differentiation. The cells were then treated with oligomycin (oligo, 1 μM) to measure the ATP turnover. The maximum respiratory capacity was assessed by addition of carbonyl cyanide 4-trifluoromethoxy phenylhydrazone (FCCP, 0.3 μM), a chemical uncoupler of electron transport and oxidative phosphorylation. The mitochondrial respiration was blocked by antimycin A (1 μM) plus rotenone (1 μM) (A + R). The oxygen consumption rate (OCR) was calculated by plotting the O_2 tension of the medium in the microenvironment above the cells as a function of time (pmol O_2/minutes).

Similar procedures were performed to measure the OCR of 3D-BA constructs to compare the metabolic function of stiff-porous vs. stiff hydrogel printing conditions.

2.10. 2-deoxy glucose uptake (2-DOG)

The engineered human 3D WA and BA constructs were tested for glucose uptake by using 2-deoxy glucose (2DOG) (Perkin Elmer) as a tracer. Prior to the glucose uptake test, the differentiated 3D-WA or BA constructs were first incubated in 6 well plates with 1 mL of serum-free low glucose DMEM, containing 1 g/L D-(+)-glucose and 20 pM human insulin for 24 h. Culture media was removed and replaced with 1 mL of HBSS buffer in the presence or absence of 100 nM human insulin for 10 min. Next, 4 nmol of [^{3}H]-2-deoxyglucose (Perkin Elmer) was added into each well. Then cellular uptakes were measured over 90 min, and the [^{3}H]-associated radioactivity was measured by a liquid scintillation counter.

2.11. Statistical analysis

All quantitative data was expressed as mean ± standard deviation (SD). Pairwise comparisons between groups were conducted using ANOVA with Scheffé post-hoc tests. A p-value of <0.05 was considered statistically significant.

3. Results

3.1. Prior exposure of human BAP to angiogenic factors promoted brown differentiation and metabolic activities.

The environmental factors that alter brown fat development in humans have not been clearly established yet. Before we used the human BAP for 3D bioprinting, we first optimized the growing conditions of BAP. Given the intimate relationship between brown adipogenesis and capillary network in vivo, we hypothesize that angiogenic factors, such as vascular endothelial growth factor (VEGF) and fibroblast growth factor 2 (FGF2), modulate brown adipogenic potential. Immortalized classical BAP from human, were pre-exposed in EGM containing VEGF and FGF2 for 48 h before brown adipogenic stimulation. Pre-exposure to EGM resulted in approximately a 10-fold increase of the brown signature gene, *Ucp1*, expression compared to BA maintained in DMEM, and a slight, but significant, increase of classical brown specific marker *Zic1* and VEGF receptor 1 (*Vegfr-R1*) (Fig. 1A). It is also notable that a robust increase of *Pgc1α*, a transcriptional regulator for mitochondrial biogenesis, and a decrease of *Hdac1*, which is a negative regulator of the brown adipocyte [42] (Fig. 1A). Consistently, there was increased UCP1 but decreased HDAC1 protein levels (Fig. 1B), suggesting that pre-exposure to EGM causes an epigenetic modification favorable to brown differentiation. In addition, pre-exposure to EGM medium robustly increased both basal- and uncoupled-respiration, determined via a Seahorse XF analyzer (Fig. 1C). To further understand the mechanism by which prior exposure to antigenic factors alters brown adipogenesis, we also examined the key miRNA regulators promoting brown transcriptional programming. As we expected, biogenesis of functional clusters of brown-specific microRNAs, i.e., miR-378, miR-30b, and miR-193b/365, were significantly higher than cells grown in the control DMEM medium (Fig. 1D). Taken together, we demonstrated that prior exposure to angiogenic environment promotes the cell-autonomous potential to convert

brown precursor cells into metabolically active human brown adipocytes via epigenetic mechanisms. By taking advantage of this pre-conditioning of BAP with angiogenic regulators, we next modulated the conditions for matrix formulation that support 3D BAT differentiation and brown function.

3.2. 3D bioprinting of WA and BA within bioinks with tunable stiffness and structure

We implemented Me-HA/Me-Gel based bioinks to encapsulate WAP and BAP and 3D bioprinted them into disc-shaped constructs. The stiffness was tuned by varying the photocrosslinking time, and the pore structure was achieved by depositing the lines with pre-designed spacing between each other (Fig. 2A). The stiffness for the constructs with 30-second photocrosslinking (soft solid) was 2.02 ± 1.11 kPa, which was significantly lower than that for 90-second photocrosslinking (9.17 ± 3.14 kPa for stiff solid, and 9.00 ± 2.38 kPa for stiff porous), regardless of the structure (Fig. 2B). Fig. 2C shows the SEM and optical images of the 3D bioprinted constructs. The hydrogel based constructs had interconnected, macro-porous structures after the ice crystals were removed by freezing and freeze drying. As expected, the pore size was larger for the soft, solid hydrogel constructs compared to their stiff counterparts. The stiff, porous constructs showed a well-maintained porous grid structure. Both encapsulated WAP and BAP showed high cell viability, with most cells stained with calcein (green) after differentiation/induction (Fig. 3A and B). In addition, the stiffness and porosity did not apparently affect cell viability (Fig. 3C). For the stiff, porous group, although some pores were blocked, probably due to hydrogel collapse, degradation, and cell confluence on the surface, most of pores were visible, which allowed for a higher surface area for nutrient transfer in the constructs (Fig. 3A and B).

3.3. Soft and porous 3D bioprinted constructs promoted white adipogenesis

Fig. 4A shows the lipid staining images from bioprinted WAP within soft or stiff bioinks with solid or porous structures. In all of the conditions, lipid production was observed around the nuclei of the cells, even in the constructs conditioned in GM. Although all of the constructs showed lipid accumulation, it seemed that the soft, 30-second crosslinked constructs, and porous constructs allowed for larger lipid droplet size and higher lipid density compared to the 90-second crosslinked constructs after induction (Fig. 4B, C). However, there was no statistic difference, based on the image analysis. In order to determine white adipogenic gene expression of 3D bioprinted WAP laden constructs, qPCR analysis was conducted after conditioning in GM or IM (Fig. 4D). The soft, solid and stiff, porous constructs in IM conditions showed the highest Pgc1α gene expression, with the soft gels being the highest. Both of these showed a significant difference between them and the GM condition. The soft, induction gels also showed significant upregulation of *Pgc1α* gene compared to stiff, induction gels. Similarly, the CCAAT/enhancer-binding protein 2 (*C/EBP-*2) gene (bio-marker for early stages of adipogenesis) expression in the soft, solid and stiff, porous gels with induction were the highest and very similar, which were significantly higher than that for soft, solid constructs in GM. The stiff, porous constructs, after induction, had the highest fatty acid binding protein 4 (*Fabp*4, late marker of adipogenesis) expression, which was significantly higher than that for soft, solid constructs in GM and stiff, solid constructs in IM.

3.4. Porous 3D bioprinted constructs promoted brown adipogenesis

Then we 3D bioprinted BAP-laden constructs with different stiffnesses and structures and conditioned them in GM or IM, similar to WAP-laden constructs, which served as a control. Fig. 5A shows the staining of lipid droplets and UCP1. In all instances, lipid production was observed around the BA, even in the GM. However, BAP-laden constructs in GM expressed very limited UCP1, while after induction, the constructs seemed to have a good amount of UCP1 production, especially for the stiff, porous constructs (Fig. 5A). QPCR results showed that the expression of cell death-inducing DFFA-like effector A (*Cidea*), which plays a role in thermo-genesis and lipolysis [43], is significantly higher in the WAP-laden constructs after induction (Fig. 5B). BA in the stiff, porous constructs showed the highest *Cidea* expression, which was statistically significant when compared to their BAP and WAP-laden counterpart constructs (Fig. 5B). All of the 3D BAP constructs showed much higher Prdm16 gene expression than their WAP counterparts, as shown in Fig. 5B. *Prdm*16 is highly enriched in BAP compared to WAP [44]. Other than the porous gels, the white adipose gels showed limited *Prdm*16 expression. The soft BAP constructs in IM had low expression, while the stiff and porous ones showed very high *Prdm*16 expression, which were significantly higher than the rest of the constructs and were similar to each other. For Ucp1 gene expression, similar to *Prdm*16, all of the WAP-laden constructs had minimal and much less *Ucp1* expression, compared to BAP laden constructs. The expression in the BAP constructs with GM conditioning was also relatively low. The other three brown adipose gel conditions had higher *Ucp1* expression, especially for soft, solid and stiff, porous constructs with induction. We also evaluated the gene expression of some inflammatory markers [i.e. interleukin 6 (*Il*6), nitric oxide synthase 2 (Nos2), Tumor necrosis factor alpha (*Tnfα*)] in the bioprinted BAP constructs after induction (Fig. 5C). The BAP in the stiff-solid constructs significantly upregulated the expression of *Il*6 and Nos2 compared to the soft-solid constructs, but their expressions were downregulated in the stiff-porous constructs. This indicates that the rigidity of the microenvironment may cause inflammatory effects, and the porous structure, with facilitated diffusion and transportation, may counteract the inflammatory effects of the rigidity of the environment.

By using these differentially bioprinted 3D BAP constructs, we next evaluated their metabolic function of by measuring 2-DOG. As we expected, 3D BAP-laden constructs showed a robustly higher glucose uptake compared to their WAP counterparts (Fig. 6A). Intriguingly, 3D cultures with soft gel conditions (i.e., 30 s UV crosslinking) showed lower glucose uptake than stiff gel conditions (90 s UV crosslinking). The same stiffness with porous structure significantly increased the 2-DOG uptake (Fig. 6A), suggesting that the stiff, porous gel group is superior to other groups for glucose uptake. In agreement with this result, the OCR was higher in 3D cultures with stiff-porous hydrogel conditions than the 3D cultures with the same stiffness without porosity modulation (Fig. 6B). Next, we examined whether increased porosity of the 3D matrix will also be beneficial for insulin-stimulated glucose uptake. Insulin stimulation (100 nM) promoted glucose uptake in both conditions of 3D BAP constructs with or without porous structure, but there was a higher magnitude with increased porosity (Fig. 6C). Collectively, these results demonstrate that metabolically active 3D bioprinted BAP constructs were achievable, and they are affected by matrix stiffness and porosity.

4. Discussion

Obesity and its related metabolic disorders, such as T2DM, are significant medical concerns due to their far reaching effects on the health of individuals and the cost of treating these health complications [45–47]. To date, there are no safe and long-lasting anti-obesity approaches, so new methods of treating obesity and its related diseases are important in the ultimate effectiveness of treatment. Utilizing BAT, which uses fats to modulate energy expenditure, might be a promising technique for treating obesity. Several studies have demonstrated that mice BAT transplantation into the visceral cavity improved glucose tolerance, increased insulin sensitivity, and lowered body weight [48,49]. In addition, Yang et al. reported that murine adipose derived stromal cells were successfully differentiated into mature adipocytes with BAT pheno-type and function within 3D hydrogels [50]. For WA, 3D culture has been demonstrated to promote adipogenesis and adipokine secretion compared to 2D culture [51,52]. It has also been demonstrated that a porous structure could improve the cell viability in vitro and promote cell ingrowth and integration in vivo [35,53]. However, it is still unclear how microenvironments affect human thermogenic brown adipogenesis and how to generate engineered BAT with clinically relevant size and function. In our current study, we first evaluated the effects of EGM medium exposure on brown adipogenesis of human BA. We then implemented 3D bioprinting to control the physicochemical properties of hydro-gel based bioinks and encapsulated both brown and white adipose cells to generate engineered constructs.

BAT is among the most vascularized tissues in the body, and the grade of vascularization determines its ability for lipid consumption and its thermogenic function [54,55]. Our current study demonstrated that exposure to EGM promoted brown adipogenesis of human BAP. Similarly, Hafner et al. demonstrated that EGM conditioning induced the formation of multilocular adipocytes and facilitated the differentiation of human induced pluripotent stem cells (hiPSC) towards brown-like adipose progenitors [56]. Most likely, VEGF in the EGM is the major stimulator, since VEGF is highly expressed in brown preadipocytes, as well as the whole BAT in murine [57,58]. In addition, VEGF had other beneficial effects on murine brown adipocytes to promote their survival, proliferation, and maintenance of mitochondria [59]. Other factors in EGM, like FGF2 and insulin-like growth factor 1, may also play an important role. Therefore, further study is required in the future to decouple the effects of different growth factors.

Compared to 2D culture systems, 3D hydrogel based culture systems better retain the characteristics of the depot of origin and promote the adipogenic differentiation of adipogenic progenitor and stromal cells [51,60]. Both HA and gelatin have been widely used as adipose tissue engineering biomaterials [24,61,62]. HA is also commonly used as a dermal and adipose filler to improve appearance and to correct deformities and loss of volume [63,64]. Our results showed that 3D Me-HA/Me-Gel hydrogel based bioinks also facilitated spontaneous adipogenesis of white and brown progenitor cells without exogenous induction. We tuned the stiffness and structure of bioprinted constructs by varying the photocrosslinking time and printing pattern. The stiffness of the soft bioprinted constructs (~2 kPa) was controlled to be within the physiological range of native adipose tissue (~2–4 kPa) [33,65], whereas the stiffness for the stiff constructs (both solid and porous, ~ 9 kPa)

was within the low range of muscle (~8–17 kPa) [66,67]. As expected, soft gel condition promoted white adipogenesis. However, for brown adipogenesis, stiff constructs promoted glucose uptake. This is probably because BA originate from the myogenic lineage of Myf5 positive progenitor cells, and thus the microenvironments with some characteristics of muscle can facilitate brown adipogenesis and subsequent metabolic activation. The porous structure increased both white and brown adipogenic gene expression and insulin mediated glucose uptake. These results demonstrated that nutrition perfusion and exchange of metabolic waste are important for adipogenic differentiation. Similarly, other studies have showed that high porosity and secondary level of pores increased adipogenic gene expression and intracellular lipid accumulation [68]. In addition, it was found that the perfusion-based culture conditions promoted faster growth of WAP and stimulated greater adipogenesis compared to static culture condition [69].

3D bioprinting allows the fabrication of constructs with arbitrary geometries and mechanical and biological heterogeneity [70,71]. Although precise geometries for adipose tissue engineering and brown fat fabrication are not necessary, the implementation of 3D bioprinting in this current study enabled the generation of a porous structure within the clinically relevant-sized constructs. In addition, 3D bioprinting supports the application of multiple cell types and bioinks by using multiple bioprinting heads. This will allow us to further incorporate other cells, like endothelial cells and other adipovascular related cells (e.g. smooth muscle cells and pericytes), to promote vascularization, since BAT is highly vascularized. For future in vivo applications, the stiffness and structure of adipose tissue constructs, as well as vascularization, should be regulated to maximize the brown adipogenic differentiation of BA and the metabolic functions of engineered BAT. Thus, 3D bioprinted BAT are promising candidates to treat obesity and other metabolism related disorders.

5. Conclusions

We pre-exposed human BAP to EGM and found that there was an increased expression of brown adipocyte markers, thus showing that it promoted their potential for conversion into metabolically active, human brown adipocytes. Once these favorable growing conditions were established, we evaluated the effect of a tunable, 3D bioprinted hydrogel matrix on encapsulated white and brown adipocytes. We 3D bioprinted the Me-HA/Me-Gel hydrogels with encapsulated WAP or BAP into soft, stiff, and stiff, porous discs. It was found that all three types had high WAP and BAP viability. For white adipogenesis, analysis using qPCR showed that the soft, solid and stiff, porous gels in IM had higher levels of white adipogenic gene expression than the stiff, solid gels and their GM counterparts. In a similar manner, we tested for brown adipogensis in the 3D bioprinted constructs. Staining showed the ability for lipid production in all of the gels, which the ones in IM having better production than the constructs in GM. Compared to the WAP laden gels, the BAP laden constructs in IM had higher levels brown adipose markers, with the bioprinted stiff and porous constructs showing the highest brown adipose gene expression and the soft constructs showing the lowest. The BAP constructs had much higher levels of glucose uptake than their WAP counterparts. The stiff BAP constructs had higher glucose uptake, with the porous ones being the highest. The constructs also supported insulin stimulated glucose uptake, and the porous structures had the highest uptake. Altogether, this work showed that the tunable, 3D bio-printed hydrogel

environments support viable adipocytes and adipogenesis, while allowing for metabolically active brown adipose constructs that are affected the matrix stiffness and porosity.

Acknowledgements

References

[1]. Wong D, Sullivan K, Heap G, The pharmaceutical market for obesity therapies, Nat. Rev. Drug Discovery 11 (2012) 669–670.22935797

[2]. Lidell ME, Betz MJ, Leinhard OD, Heglind M, Elander L, Slawik M, Mussack T, Nilsson D, Romu T, Nuutila P, Virtanen KA, Beuschlein F, Persson A, Borga M, Enerbäck S, Evidence for two types of brown adipose tissue in humans, Nat. Med 19 (2013) 631–634.23603813

[3]. Chondronikola M, Volpi E, Børsheim E, Porter C, Annamalai P, Enerbäck S, Lidell ME, Saraf MK, Labbe SM, Hurren NM, Yfanti C, Chao T, Andersen CR, Cesani FI, Hawkins H, Sidossis LS, Brown adipose tissue improves whole-body glucose homeostasis and insulin sensitivity in humans, Diabetes 63 (2014) 4089–4099.25056438

[4]. Poher AL, Altirriba J, Veyrat-Durebex C, Rohner-Jeanrenaud F, Brown adipose tissue activity as a target for the treatment of obesity/insulin resistance, Front. Physiol 6 (2015) 004.

[5]. Yoneshiro T, Aita S, Matsushita M, Kayahara T, Kameya T, Kawai Y, Iwanaga T, Saito M, Recruited brown adipose tissue as an antiobesity agent in humans, J. Clin. Investig 123 (2013) 3404–3408.23867622

[6]. Lee P, Werner CD, Kebebew E, Celi FS, Functional thermogenic beige adipogenesis is inducible in human neck fat, Int. J. Obesity 2014 (38) (2005) 170–176.

[7]. Zingaretti MC, Crosta F, Vitali A, Guerrieri M, Frontini A, Cannon B, Nedergaard J, Cinti S, The presence of UCP1 demonstrates that metabolically active adipose tissue in the neck of adult humans truly represents brown adipose tissue, FASEB J 23 (2009) 3113–3120.19417078

[8]. Ouellet V, Labbe SM, Blondin DP, Phoenix S, Guerin B, Haman F, Turcotte EE, Richard D, Carpentier AC, Brown adipose tissue oxidative metabolism contributes to energy expenditure during acute cold exposure in humans, J. Clin. Invest 122 (2012) 545–552.22269323

[9]. Sidossis L, Kajimura S, Brown and beige fat in humans: thermogenic adipocytes that control energy and glucose homeostasis, J. Clin. Invest 125 (2015) 478–486.25642708

[10]. Orava J, Nuutila P, Noponen T, Parkkola R, Viljanen T, Enerback S, Rissanen A, Pietilainen KH, Virtanen KA, Blunted metabolic responses to cold and insulin stimulation in brown adipose tissue of obese humans, Obesity (Silver Spring, Md) 21 (2013) 2279–2287.

[11]. Vosselman MJ, van der Lans AA, Brans B, Wierts R, van Baak MA, Schrauwen P, van Marken Lichtenbelt WD, Systemic beta-adrenergic stimulation of thermogenesis is not accompanied by brown adipose tissue activity in humans, Diabetes 61 (2012) 3106–3113.22872233

[12]. Saito M, Okamatsu-Ogura Y, Matsushita M, Watanabe K, Yoneshiro T, Nio-Kobayashi J, Iwanaga T, Miyagawa M, Kameya T, Nakada K, Kawai Y, Tsujisaki M, High incidence of metabolically active brown adipose tissue in healthy adult humans: effects of cold exposure and adiposity, Diabetes 58 (2009) 1526–1531.19401428

[13]. Vijgen GHEJ, Bouvy ND, Teule GJJ, Brans B, Schrauwen P, van Marken Lichtenbelt WD, Brown adipose tissue in morbidly obese subjects, PLoS One 6 (2011) e17247.21390318

[14]. Yoneshiro T, Aita S, Matsushita M, Kameya T, Nakada K, Brown adipose tissue, whole-body energy expenditure, and thermogenesis in healthy adult men, Obesity 19 (2011) 13–16.20448535

[15]. Lee HM, Kim JJ, Kim HJ, Shong M, Ku BJ, Jo EK, Upregulated NLRP3 inflammasome activation in patients with type 2 diabetes, Diabetes 62 (2013) 194–204.23086037

[16]. Vandanmagsar B, Youm YH, Ravussin A, Galgani JE, Stadler K, Mynatt RL, Ravussin E, Stephens JM, Dixit VD, The NLRP3 inflammasome instigates obesity-induced inflammation and insulin resistance, Nat. Med 17 (2011) 179–188.21217695

[17]. Stienstra R, van Diepen JA, Tack CJ, Zaki MH, van de Veerdonk FL, Perera D, Neale GA, Hooiveld GJ, Hijmans A, Vroegrijk I, van den Berg S, Romijn J, Rensen PC, Joosten LA, Netea MG, Kanneganti TD, Inflammasome is a central player in the induction of obesity and insulin resistance, Proc. Natl. Acad. Sci. U.S.A 108 (2011) 15324–15329.21876127

[18]. Holmes D, PCOS: Benefits of brown adipose tissue transplantation, Nat. Rev. Endocrinol (2016).

[19]. Liu X, Wang S, You Y, Meng M, Zheng Z, Dong M, Lin J, Zhao Q, Zhang C, Yuan X, Hu T, Liu L, Huang Y, Zhang L, Wang D, Zhan J, Jong Lee H, Speakman JR, Jin W, Brown adipose tissue transplantation reverses obesity in Ob/Ob mice, Endocrinology 156 (2015) 2461–2469.25830704

[20]. Park A, Kim WK, Bae KH, Distinction of white, beige and brown adipocytes derived from mesenchymal stem cells, World J. Stem Cells 6 (2014) 33–42.24567786

[21]. Kajimura S, Saito M, A new era in brown adipose tissue biology: molecular control of brown fat development and energy homeostasis, Annu. Rev. Physiol 76 (2014) 225–249.24188710

[22]. Holmes D, Adipose tissue: New route to functional human beige adipocytes, Nat. Rev. Endocrinol 13 (2017) 251.

[23]. Kiefer FW, The significance of beige and brown fat in humans, Endocrine Connections 6 (2017) R70–R79.28465400

[24]. Huber B, Borchers K, Tovar GEM, Kluger PJ, Methacrylated gelatin and mature adipocytes are promising components for adipose tissue engineering, J. Biomater. Appl 30 (2016) 699–710.26017717

[25]. Clevenger TN, Hinman CR, Ashley Rubin RK, Smither K, Burke DJ, Hawker CJ, Messina D, Van Epps D, Clegg DO, Vitronectin-based, biomimetic encapsulating hydrogel scaffolds support adipogenesis of adipose stem cells, Tissue Eng. Part A 22 (2016) 597–609.26956095

[26]. Korurer E, Kenar H, Doger E, Karaoz E, Production of a composite hyaluronic acid/gelatin blood plasma gel for hydrogel-based adipose tissue engineering applications, J. Biomed. Mater. Res. Part A 102 (2014) 2220–2229.

[27]. Pellegrinelli V, Heuvingh J, Du Roure O, Rouault C, Devulder A, Klein C, Lacasa M, Clément E, Lacasa D, Clément K, Human adipocyte function is impacted by mechanical cues, J. Pathol 233 (2014) 183–195.24623048

[28]. Okla M, Ha JH, Temel RE, Chung S, BMP7 drives human adipogenic stem cells into metabolically active beige adipocytes, Lipids 50 (2015) 111–120.25534037

[29]. Tharp KM, Jha AK, Kraiczy J, Yesian A, Karateev G, Sinisi R, Dubikovskaya EA, Healy KE, Stahl A, Matrix-assisted transplantation of functional beige adipose tissue, Diabetes 64 (2015) 3713–3724.26293504

[30]. Loh RKC, Kingwell BA, Carey AL, Human brown adipose tissue as a target for obesity management; beyond cold-induced thermogenesis, Obes. Rev 18 (2017) 1227–1242.28707455

[31]. Park J, Kim M, Sun K, An YA, Gu X, Scherer PE, VEGF-A-expressing adipose tissue shows rapid beiging and enhanced survival after transplantation and confers IL-4-independent metabolic improvements, Diabetes 66 (2017) 1479–1490.28254844

[32]. Min SY, Kady J, Nam M, Rojas-Rodriguez R, Berkenwald A, Kim JH, Noh HL, Kim JK, Cooper MP, Fitzgibbons T, Brehm MA, Corvera S, Human 'brite/beige' adipocytes develop from capillary networks, and their implantation improves metabolic homeostasis in mice, Nat. Med 22 (2016) 312–318.26808348

[33]. Young DA, Choi YS, Engler AJ, Christman KL, Stimulation of adipogenesis of adult adipose-derived stem cells using substrates that mimic the stiffness of adipose tissue, Biomaterials 34 (2013) 8581–8588.23953825

[34]. Shoham N, Girshovitz P, Katzengold R, Shaked NT, Benayahu D, Gefen A, Adipocyte stiffness increases with accumulation of lipid droplets, Biophys. J 106 (2014) 1421–1431.24655518

[35]. Chung HJ, Park TG, Injectable cellular aggregates prepared from biodegradable porous microspheres for adipose tissue engineering, Tissue Eng. Part A 15 (2009) 1391–1400.19327016

[36]. Xue R, Lynes MD, Dreyfuss JM, Shamsi F, Schulz TJ, Zhang H, Huang TL, Townsend KL, Li Y, Takahashi H, Weiner LS, White AP, Lynes MS, Rubin LL, Goodyear LJ, Cypess AM, Tseng YH, Clonal analyses and gene profiling identify genetic biomarkers of the thermogenic potential of human brown and white preadipocytes, Nat. Med 21 (2015) 760–768.26076036

[37]. Duan B, Yin ZY, Kang LH, Magin RL, Butcher JT, Active tissue stiffness modulation controls valve interstitial cell phenotype and osteogenic potential in 3D culture, Acta Biomater 36 (2016) 42–54.26947381

[38]. Kuss MA, Harms R, Wu S, Wang Y, Untrauer JB, Carlson MA, Duan B, Short-term hypoxic preconditioning promotes prevascularization in 3D bioprinted bone constructs with stromal vascular fraction derived cells, RSC Adv 7 (2017) 29312–29320.28670447

[39]. Duan B, Hockaday LA, Kapetanovic E, Kang KH, Butcher JT, Stiffness and adhesivity control aortic valve interstitial cell behavior within hyaluronic acid based hydrogels, Acta Biomater 9 (2013) 7640–7650.23648571

[40]. Okla M, Wang W, Kang I, Pashaj A, Carr T, Chung S, Activation of Toll-like receptor 4 (TLR4) attenuates adaptive thermogenesis via endoplasmic reticulum stress, J. Biol. Chem 290 (2015) 26476–26490.26370079

[41]. Kim J, Okla M, Erickson A, Carr T, Natarajan SK, Chung S, Eicosapentaenoic acid potentiates brown thermogenesis through FFAR4-dependent up-regulation of miR-30b and miR-378, J. Biol. Chem 291 (2016) 20551–20562.27489163

[42]. Li F, Wu R, Cui X, Zha L, Yu L, Shi H, Xue B, Histone deacetylase 1 (HDAC1) negatively regulates thermogenic program in brown adipocytes via coordinated regulation of histone H3 lysine 27 (H3K27) deacetylation and methylation, J. Biol. Chem 291 (2016) 4523–4536.26733201

[43]. Chan SC, Lin SC, Li P, Regulation of Cidea protein stability by the ubiquitin-mediated proteasomal degradation pathway, Biochem. J 408 (2007) 259–266.17711404

[44]. Seale P, Kajimura S, Yang W, Chin S, Rohas LM, Uldry M, Tavernier G, Langin D, Spiegelman BM, Transcriptional control of brown fat determination by PRDM16, Cell Metab 6 (2007) 38–54.17618855

[45]. Chen L, Magliano DJ, Zimmet PZ, The worldwide epidemiology of type 2 diabetes mellitus – present and future perspectives, Nat. Rev. Endocrinol 8 (2012) 228–236.

[46]. Zimmet P, Alberti KGMM, Shaw J, Global and societal implications of the diabetes epidemic, Nature 414 (2001) 782–787.11742409

[47]. Johnston CA, Moreno JP, Foreyt JP, Cardiovascular effects of intensive lifestyle intervention in type 2 diabetes, Curr. Atheroscler. Rep 16 (2014) 457.25288176

[48]. Stanford KI, Middelbeek RJW, Townsend KL, An D, Nygaard EB, Hitchcox KM, Markan KR, Nakano K, Hirshman MF, Tseng YH, Goodyear LJ, Brown adipose tissue regulates glucose homeostasis and insulin sensitivity, J. Clin. Investig 123 (2013) 215–223.23221344

[49]. Liu X, Zheng Z, Zhu X, Meng M, Li L, Shen Y, Chi Q, Wang D, Zhang Z, Li C, Li Y, Xue Y, Speakman JR, Jin W, Brown adipose tissue transplantation improves whole-body energy metabolism, Cell Res 23 (2013) 851–854.23649313

[50]. Yang JP, Anderson AE, McCartney A, Ory X, Ma G, Pappalardo E, Bader J, Elisseeff JH, Metabolically active three-dimensional brown adipose tissue engineered from white adipose-derived stem cells, Tissue Eng. Part A 23 (2017) 253–262.28073315

[51]. Emont MP, Yu H, Jun H, Hong X, Maganti N, Stegemann JP, Wu J, Using a 3D culture system to differentiate visceral adipocytes in vitro, Endocrinology 156 (2015) 4761–4768.26425808

[52]. Klingelhutz AJ, Gourronc FA, Chaly A, Wadkins DA, Burand AJ, Markan KR, Idiga SO, Wu M, Potthoff MJ, Ankrum JA, Scaffold-free generation of uniform adipose spheroids for metabolism research and drug discovery, Sci. Rep 8 (2018) 523.29323267

[53]. Patrick CW, Tissue engineering strategies for adipose tissue repair, Anat. Rec 263 (2001) 361–366.11500812

[54]. Shimizu I, Aprahamian T, Kikuchi R, Shimizu A, Papanicolaou KN, MacLauchlan S, Maruyama S, Walsh K, Vascular rarefaction mediates whitening of brown fat in obesity, J. Clin. Investig 124 (2014) 2099–2112.24713652

[55]. Cao Y, Adipose tissue angiogenesis as a therapeutic target for obesity and metabolic diseases, Nat. Rev. Drug Discovery 9 (2010) 107–115.20118961

[56]. Hafner AL, Contet J, Ravaud C, Yao X, Villageois P, Suknuntha K, Annab K, Peraldi P, Binetruy B, Slukvin II, Ladoux A, Dani C, Brown-like adipose progenitors derived from human induced pluripotent stem cells: Identification of critical pathways governing their adipogenic capacity, Sci. Rep 6 (2016) 32490.27577850

[57]. Tonello C, Giordano A, Cozzi V, Cinti S, Stock MJ, Carruba MO, Nisoli E, Role of sympathetic activity in controlling the expression of vascular endothelial growth factor in brown fat cells of lean and genetically obese rats, FEBS Lett 442 (1999) 167–172.9928995

[58]. Asano A, Irie Y, Saito M, Isoform-specific regulation of vascular endothelial growth factor (VEGF) family mRNA expression in cultured mouse brown adipocytes, Mol. Cell. Endocrinol 174 (2001) 71–76.11306173

[59]. Bagchi M, Kim LA, Boucher J, Walshe TE, Kahn CR, D'Amore PA, Vascular endothelial growth factor is important for brown adipose tissue development and maintenance, FASEB J 27 (2013) 3257–3271.23682123

[60]. Kokai LE, Marra KG, Kershaw EE, Three-dimensional adipocyte culture: the next frontier for adipocyte biology discovery, Endocrinology 156 (2015) 4375–4376.26492473

[61]. Knopf-Marques H, Pravda M, Wolfova L, Velebny V, Schaaf P, Vrana NE, Lavalle P, Hyaluronic acid and its derivatives in coating and delivery systems: applications in tissue engineering, regenerative medicine and immunomodulation, Adv. Healthcare Mater 5 (2016) 2841–2855.

[62]. Kessler L, Gehrke S, Winnefeld M, Huber B, Hoch E, Walter T, Wyrwa R, Schnabelrauch M, Schmidt M, Kückelhaus M, Lehnhardt M, Hirsch T, Jacobsen F, Methacrylated gelatin/hyaluronan-based hydrogels for soft tissue engineering, J. Tissue Eng (2017).

[63]. Zhu Y, Crewe C, Scherer PE, Hyaluronan in adipose tissue: beyond dermal filler and therapeutic carrier, Sci. Transl. Med 8 (2016). 323ps4.

[64]. Greene JJ, Sidle DM, The hyaluronic acid fillers. Current understanding of the tissue device interface, Facial Plastic Surg. Clin. North Am 23 (2015) 423–432.

[65]. Wen JH, Vincent LG, Fuhrmann A, Choi YS, Hribar KC, Taylor-Weiner H, Chen S, Engler AJ, Interplay of matrix stiffness and protein tethering in stem cell differentiation, Nat. Mater 13 (2014) 979–987.25108614

[66]. Engler AJ, Griffin MA, Sen S, Bönnemann C, Sweeney HL, Discher DE. Myotubes differentiate optimally on substrates with tissue-like stiffness. Proceedings of the 2005 Summer Bioengineering Conference 2005;2005:307–9.

[67]. Lee S, Serpooshan V, Tong X, Venkatraman S, Lee M, Lee J, Chirikian O, Wu JC, Wu SM, Yang F, Contractile force generation by 3D hiPSC-derived cardiac tissues is enhanced by rapid establishment of cellular interconnection in matrix with muscle-mimicking stiffness, Biomaterials 131 (2017) 111–120.28384492

[68]. Yu C, Bianco J, Brown C, Fuetterer L, Watkins JF, Samani A, Flynn LE, Porous decellularized adipose tissue foams for soft tissue regeneration, Biomaterials 34 (2013) 3290–3302.23384795

[69]. Liu Y, Kongsuphol P, Gourikutty SBN, Ramadan Q, Human adipocyte differentiation and characterization in a perfusion-based cell culture device, Biomed. Microdev 19 (2017) 18.

[70]. Mosadegh B, Xiong GL, Dunham S, Min JK, Current progress in 3D printing for cardiovascular tissue engineering, Biomed. Mater 10 (2015) 034002.25775166

[71]. Kang HW, Lee SJ, Ko IK, Kengla C, Yoo JJ, Atala A, A 3D bioprinting system to produce human-scale tissue constructs with structural integrity, Nat. Biotechnol 34 (2016) 312–319.26878319

Statement of Significance

One promising strategy for the treatment or prevention of obesity-mediated health complications is augmenting brown adipose tissues (BAT), which is a specialized fat that actively dissipate energy in the form of heat and maintain energy balance. In this study, we determined how pre-exposing human brown adi-pose progenitors (BAP) to angiogenic factors in 2D and how bioprinted microenvironments in 3D affected brown adipogenic differentiation and metabolic activity. We demonstrated that white and brown adipo-genesis, and thermogenesis were regulated by tuning the bioprintable matrix stiffness and construct structure. This study not only unveils the interaction between BAP and 3D physiological microenvironments, but also presents a novel tissue engineered strategy to manage obesity and other related metabolic disorders.
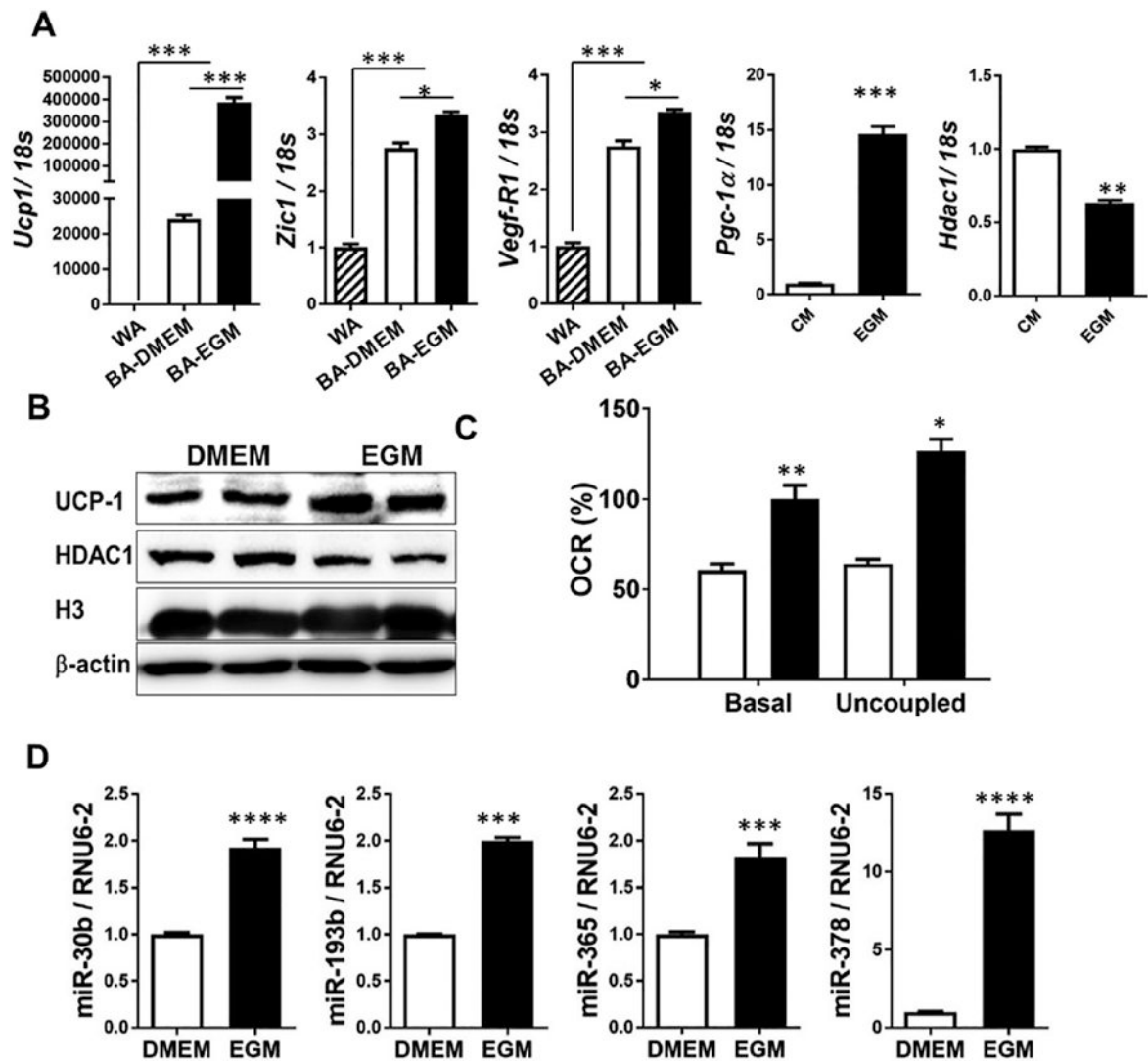
Fig. 1.
Pre-exposure to angiogenic factors promoted the brown-adipogenic potential of human BAP.
(A) qPCR analysis of *Ucp1*, *Zic1*, *Vegfr1*, *Pgc1a and Hdac1*; (B) Protein levels of UCP1, HDAC1, histone3, and α-actin as a loading control (n = 4 per group); (C) Oxygen consumption rate (OCR) by Seahorse XF analyzer; (D) Brown-specific miRNA levels of miR-30b, 193b, 365 and 378. U6 small nuclear RNA2 (RNU6–2) was used as a reference (n = 4–5 per group), *p < 0.05, **p < 0.01, ***p < 0.001, ****p < 0.0001.
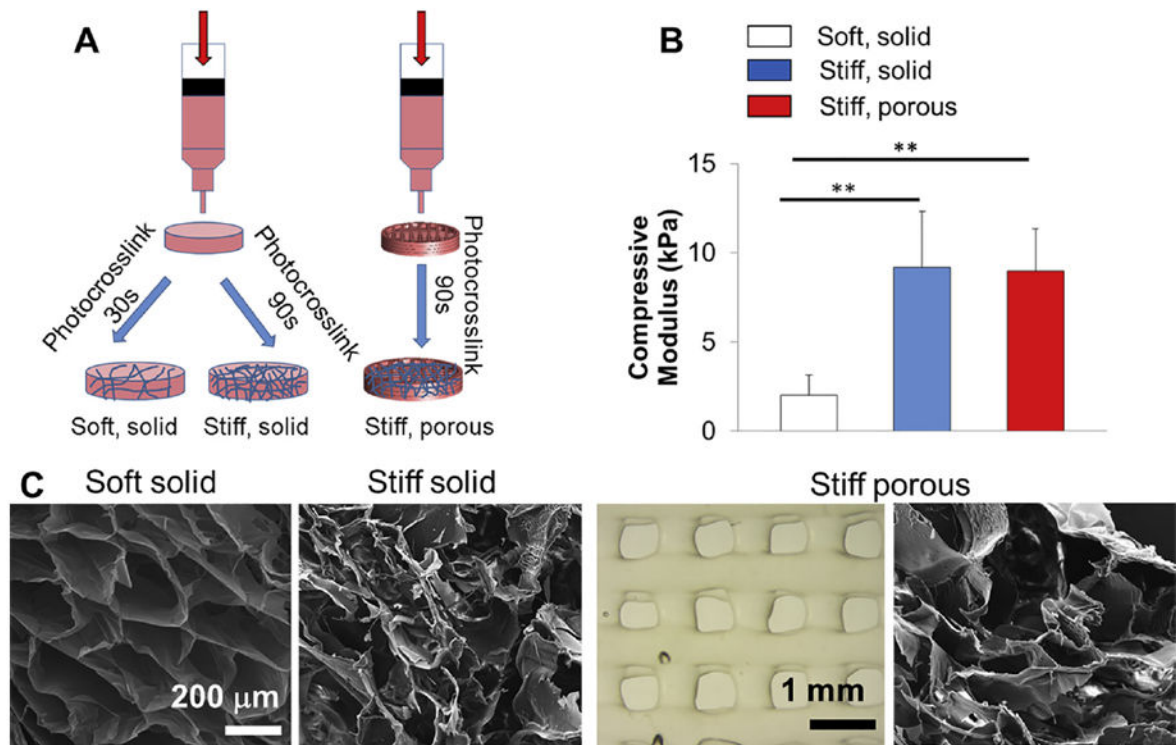
Fig. 2.
The tunability of the bioprinted hydrogel constructs allows for varying physical properties and surface areas. (A) Multiple bioprinting patterns and crosslinking times creates different geometry and stiffness (Soft = UV crosslinking for 30 s, Stiff = UV crosslinking for 90 s, Solid = bioprinted constructs with solid structure, Porous = bioprinted constructs with porous structure); (B) Compressive modulus of the different hydrogel constructs; n = 5–6; **$p < 0.01$; (C) Typical SEM and optical micrographs.
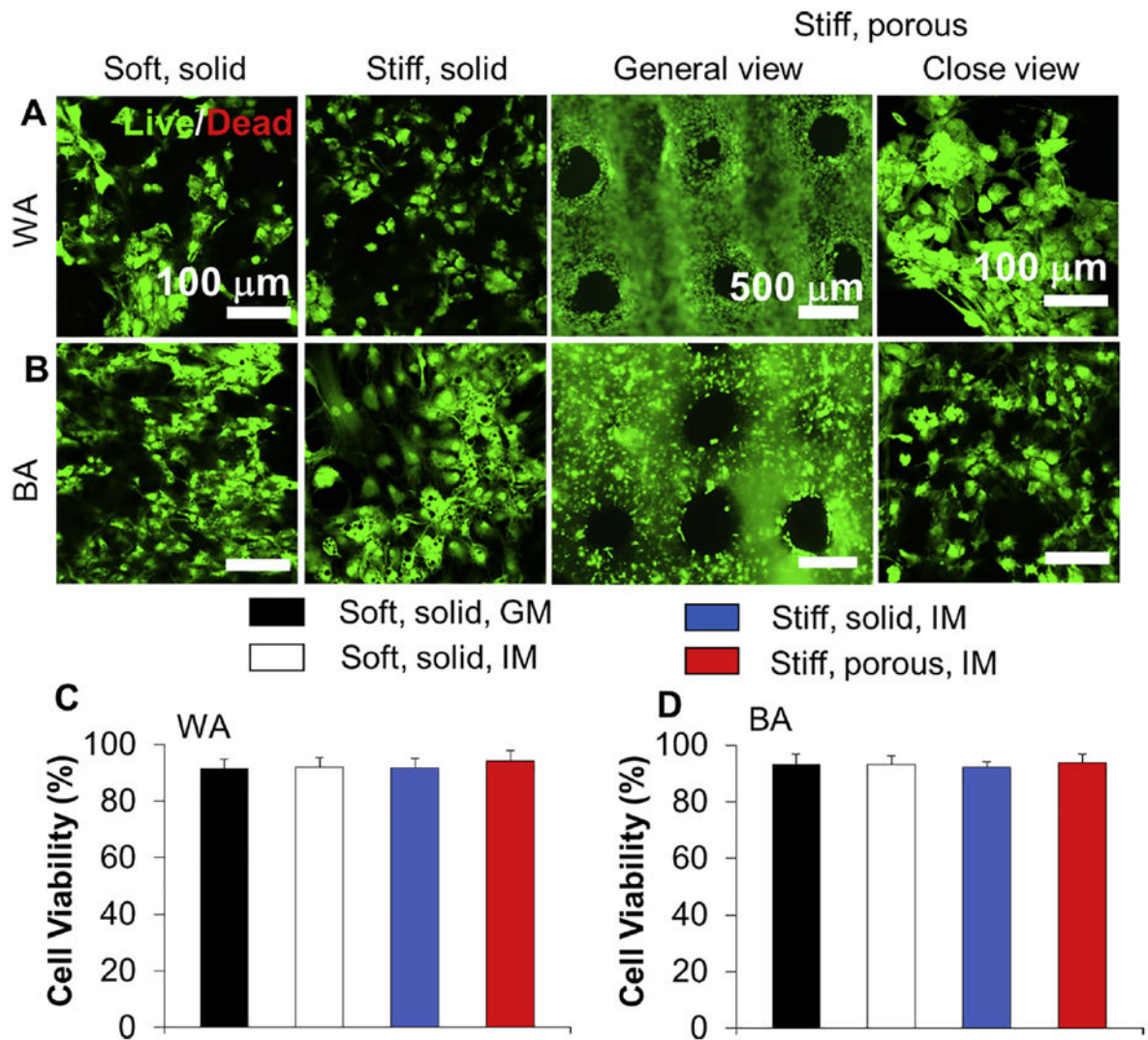
Fig. 3.
Live/dead staining of the three types of hydrogel constructs shows the cell viability after induction. (A) Hydrogel constructs with WAP encapsulated; (B) Hydrogel constructs with BAP encapsulated; (C) Semi-quantitative measurement of cell viability based on Live/Dead images (n = 6).
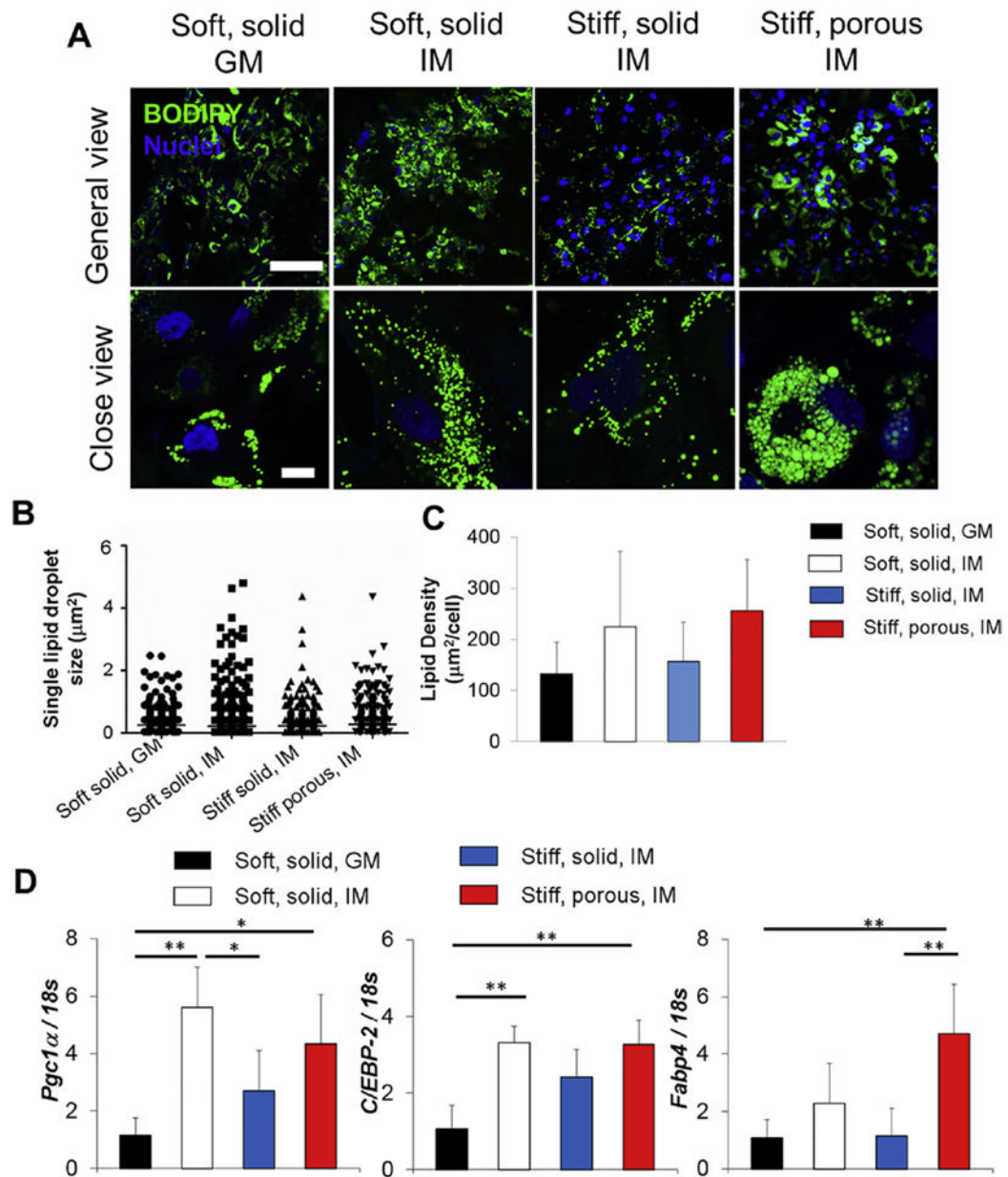
Fig. 4.
Lipid production of white adipocytes across all constructs in IM and soft constructs in GM. (A) Bodipy staining for lipids and nuclear staining (scale bar, 100 μm); (B) Size and size distribution of the single lipid droplets; (more than 100 lipid droplets from at least three IF images); (C) Lipid density (calculated by comparing total lipid area with total cells in the images, n = 5–6 images); (D) qPCR analysis of white adipogenesis related genes expression. Relative gene expression is presented as normalized to 18S and expressed relative to soft, solid constructs in GM. (n = 3, *p < 0.05, **p < 0.01).
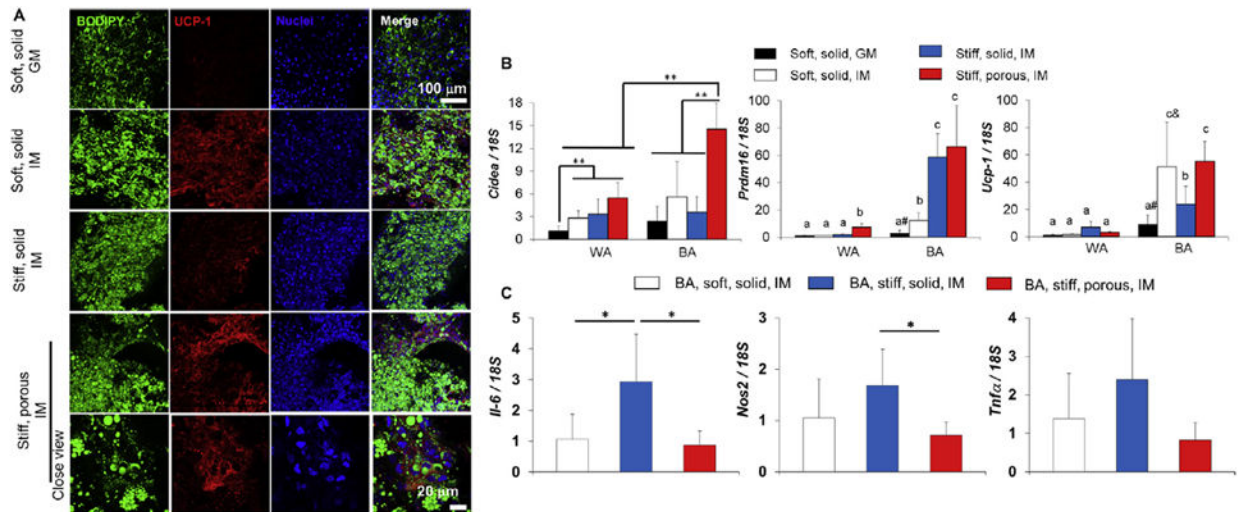
Fig. 5.
Staining and gene expression across all constructs in IM and soft constructs in GM. (A) Staining of brown adipose constructs. Bodipy staining for lipids, UCP-1 staining for a brown adipogenic marker, and nuclear staining; (B, C) qPCR analysis of brown adipogenesis and inflammation related genes expression. (B) Relative gene expression is presented as normalized to 18 s and expressed relative to soft, solid constructs with WA in GM. (n = 3, bars that do not share letters are significantly different from each other, **p < 0.01, # indicates p < 0.05 comparing to soft, solid constructs with WA, & indicates no significant difference comparing to stiff, solid constructs with BA); (C) Relative gene expression is presented as normalized to 18 s and expressed relative to soft, solid constructs with BA in IM. (n = 3, *p < 0.05).
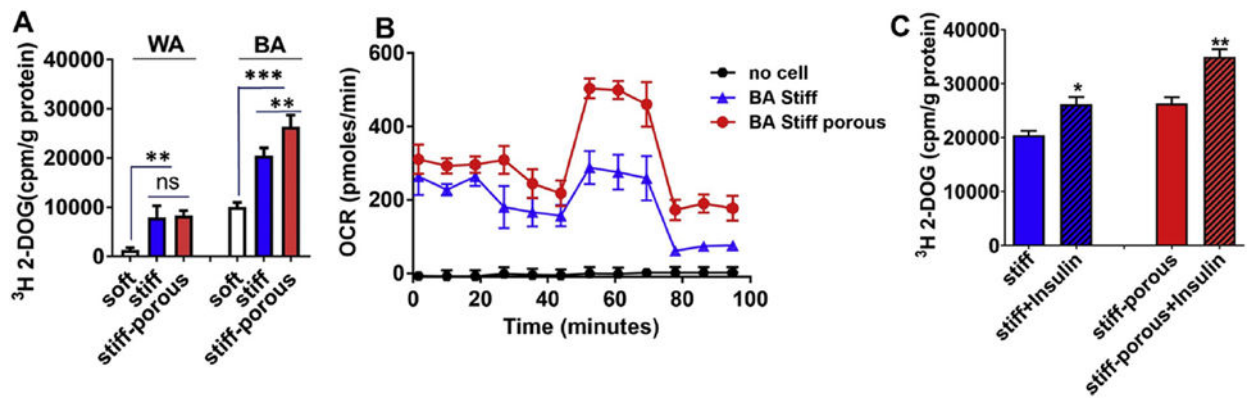
Fig. 6.
Hydrogel stiffness and porosity altered metabolic function of 3D bioprinted BAP laden constructs. Roughly 5×10^6 of WAP and BAP were bioprinted in differential bioink and bioprinting structure conditions. Glucose uptake was measured by using ^{3}H-2-deoxy glucose (DOG) as a metabolic tracer. (A) Basal levels of 2-DOG uptake in WA and BA cultures; (n = 4, **p < 0.01, ***p < 0.001), (B) Oxygen consumption rate in BA cultures in stiff or stiff-porous hydrogel scaffolds (n = 4 per group). No cell control was used as a negative control. (C) 2-DOG uptake in the presence and absence of insulin (100 nM) for 90 min. Data normalized by protein levels and expressed as cpm/g protein/per 3D bioprinted construct (n = 4, *p < 0.05, **p < 0.01).